Chapter

Modelling of Photonic Crystal (PhC) Cavities: Theory and Applications

Ahmad Rifqi Md Zain and Richard M. De La Rue

Abstract

In recent years, many researchers have shown their interest in producing a compact high-performance optical chip that is useful for most telecommunication applications. One of the solutions is by realising photonic crystal (PhC) structures that exhibit high-quality factors in a small mode volume, V. Silicon on insulator (SOI) is one of the main contenders due to its high-index contrast between the silicon (Si) core waveguide with silica (SiO_2) cladding surrounding it. The maturity of silicon photonic can also be incorporated with CMOS chips making it a desired material. A strong optical confinement provided by PhC structures makes it possible to realise the compact device on a single chip. In this chapter, we will discuss a fundamental background of photonic crystal cavities mainly on one-dimensional (1D) structures, which are the simplest as compared to their counterparts, 2D and 3D PhC device structures. We have modelled a photonic crystal cavity using finite-difference time-domain (FDTD) approach. This approach uses time-dependent Maxwell equation to cover wide frequency range in a single simulation. The results are then compared with the actual measured results showing a significant agreement between them. The design will be used as basic building block for designing a more complex PhC structures that exhibit high-quality factors for applications such as filtering, DWDM and sensors.

Keywords: photonic crystal (PhC), photonic wire (PhW), integrated optics, high-quality factors, finite-difference time-domain (FDTD)

1. Introduction

The potential importance of integrated optics was not fully realised until 1968. Light propagation in thin films has been proposed and developed extensively since then [1]. The term integrated optics relates to a wide variety of structures where the propagation of light is controlled by a thin dielectric film or by strips of dielectric. The range of laser frequencies available and the types of material used have their limitations. Initially, gas laser and solid-state lasers were used as the light sources in early experiments. There is a possible need for much smaller sources that can be used to achieve the requirement of integrated optics in order to integrate with other applications. For wavelengths smaller than a certain value, say around 0.1 μm, overcoming large absorption and scattering losses becomes a priority since the smaller wavelength range imposes limitations on the practical use of waveguiding.

In addition, waveguide integrated optics is based on electromagnetic waveguiding at optical frequencies using thin-film optics. In recent years, semiconductor devices have played a major role in the evolution of integrated optics, due to their significant properties relevant to the goal of monolithic integrated optical circuits. In the early 1960s, research on thin-film phenomena became the key route towards developing more complex waveguide properties. The guiding action of planar layers in p-n junctions was observed and reported in 1963 by Yariv and Leite [2] and Bond et al. [3]. Their result has been subsequently used by Nelson and Reinhardt [4] in providing light modulation via the electro-optic effect. Although there was no concern with the optical waveguide circuitry, this work was just the beginning of the new era of planar thin-film waveguides. Light propagation in thin films has been proposed and developed since then [5]. The subject of dielectric periodic microstructures has become a priority ever since the evolution of lasers and integrated optics generally in the early 1960s [5–11]. This great evolution was just the beginning of the new era of development of photonic microstructures on single compact chips. Much research has been carried out with the aim of providing faster optical communication and data processing—whether for entertainment, route switching or computational purposes. In recent years, the motivation towards producing compact and faster communication has become a platform for much research, including switching purposes.

In addition, the advance in photonic technology for many applications has emerged on a large scale, whether using active devices such as III–V semiconductor materials or even silicon and silica passive devices. But the latter two materials still work as a separate system, although the main aim is still to achieve a monolithic photonic integration that is capable of handling any application in a single chip. The developments based on the concepts formulated by Purcell [12, 13] regarding the effect of radiation properties due to the presence of mirrors have been discussed extensively. These ideas led to the new concept of photonic crystals (PhCs) [14, 15]. Instead of manipulating the electrons that are involved in the use of the conventional electronic properties of solids, where they can produce an electronic band gap, photons are manipulated in periodic structures (photonic crystals)—and can exhibit stopband and photonic band-gap behaviour. In other words, photons are not allowed to propagate through the 'crystal' structures at all—and there can be a forbidden gap or band gap.

Much of the attraction in the research areas of the micro- and nanophotonic structures comes from the use of high refractive index contrast materials such as silicon-on-insulator (SOI) that have been increasingly used in recent years. This development is due to the ability of silicon technology to support monolithic integration of optical interconnects and form fully functional photonic devices that can be incorporated into CMOS chips. Soref and Lorenzo [16] have demonstrated the possibilities of passive and active silicon waveguides as long ago as 1985, with single-crystal silicon grown epitaxially on a heavily doped silicon substrate. The advances of silicon-based and silicon-on-insulator optoelectronics have also been noted by Jalali et al. [17] and Masini et al. [18].

2. Photonic crystal and photonic wire waveguides

The concept of photonic band-gap structures was independently proposed by John [14] and by Yablonovitch [15]. PBG structures create the condition where over a certain photon energy range, light can travel through the periodic structure—and is reflected back when impinging onto the crystal and is not allowed to propagate—thus creating a so-called forbidden zone. In 1991, the first experimental

demonstrations have shown that by using an array of holes drilled into the high refractive index material, a stopband is produced where no transmission is allowed over this frequency range [19]. Full PBG structures consist of three-dimensionally periodic structures that inhibit spontaneous emission within the electromagnetic band gap. New design has been developed and innovated based on this concept ever since, although improving the overall performance of this device is still a major concern for full device functionality—and there is also a performance limitation determined by various fabrication processes [19, 20]. 3D photonic crystal structures (PhCs) are one of the possible contenders for the provision of highly compact devices on a single chip that will allow the realisation of complex subsystems. Due to the inherent difficulties of realising and controllably modifying 3D structures, work on 2D and 1D structures has emerged tremendously—which is partly due to the lesser design complexity and the reduction in size. But they can produce some interesting results that have contributed significantly towards the realisation of photonic integrated circuits (PICs). The motivation towards miniaturising PIC devices has expanded the need to put more effort into designing compact photonic crystal-based devices. The massive development of telecommunication infrastructures has created a large demand of multiple applications on a single chip by using a combination of several optical subsystems.

In general, photonic crystal device structures exhibit a strong optical confinement covering a fairly large frequency spectrum. Strong optical confinement is needed in a small volume to provide a suitable platform in the optical emission properties—thus creating enhancement of the luminescent 'atoms' through spontaneous emission. By creating a 'defect' or a small region surrounded by the photonic crystal arrangement, the basic properties of that photonic crystal lattice are significantly changed. In other words, the photonic crystal has the capability to localise light when a 'defect' is introduced within the periodicity of the crystal arrangement —thus forming a micro-cavity that is surrounded by a highly reflective mirror region. For example, in 2D photonic crystal structures, a 'defect' or micro-cavity can be formed by simply removing one or more holes [21–23]—or by changing the surrounding hole sizes [24–26]. Light that is strongly confined within the channel waveguide formed by the photonic crystal arrangement (square [27] or hexagonal lattice [28, 29] is directly coupled into the micro-cavity region. In this design arrangement, light may be guided through the structure by removing a single row of holes to form a channel waveguide—and in this way, light can propagate at the characteristic frequency of the cavity, within the band gap. Channel waveguides may be designed to have different widths, W, such as W1 [30]—where a single row of holes is removed to provide a channel waveguide. In other examples, W3 [31] consists of three hole removed and W0.7 [32]—i.e. a situation where the spacing between two blocks of photonic crystal is additionally increased by 0.7 of a lattice spacing. Recently, low propagation losses, 4.1 dB/cm, have been obtained in a single-line defect W1 PhC channel waveguide [33] which shows that PhCs can provide a suitable platform for designing low loss devices. In 1D photonic crystal structures, the micro-cavity has great potential for producing a high-quality factor in a small volume—thus providing a suitable platform to design a wavelength selective device, for example, for WDM applications using passive components such as multiplexers/de-multiplexers, optical switching, sensors and optical filters. On the other hand, in 1D photonic crystals, micro-cavities may be formed by creating a defect and using a smaller hole in the middle of a single-row crystal, as shown in **Figure 1**.

In photonic crystal (PhC) micro-cavity structures, the optical properties may be characterised by the Q/V ratio (often called the Purcell factor [12, 13]), where Q is the quality factor and V is the modal volume corresponding to the particular

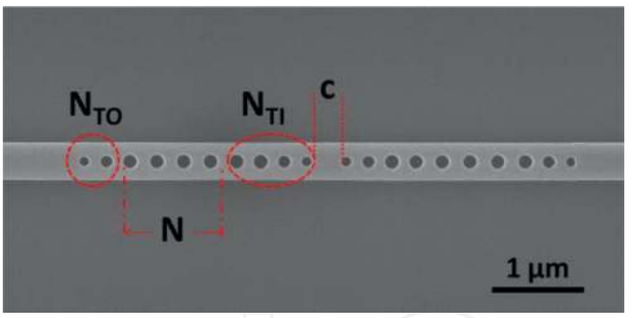

Figure 1.
1D PhC/PhW waveguide structures with a series of PhC hole of periodic spacing, a, and hole diameter, d, embedded in 500 nm wire. The tapered hole introduced has a number of hole tapered outside cavity, N_{TO}, and the number of tapered hole within cavity, N_{TI}, with cavity length, c. A periodic mirror has N number of equally spaced hole.

micro-cavity and its characteristic electromagnetic resonant modes. Thus designing high Q-factor optical micro-cavities confined in a small volume, V, may be useful for high-speed optical processing—where light is confined within a small volume on the order of $(\lambda/2n)^3$—and λ is the emission wavelength and n is the refractive index of the given material. Recently, designing ultrasmall micro-cavity devices based on 1D PhC/PhW dimensions has been of major interest because of their capability to provide extremely high Q/V values, close to the theoretical values of the modal volume, $V = (\lambda/2n)^3$. Q-factor values as large as 10^8 have been achieved, but this experimental value was based on silica toroids [34]—but this design has a relatively large modal volume, corresponding to a Q/V value of approximately 5×10^4 $(\lambda/2n)$.

Therefore, in most optical telecommunication applications, there is a need to have 1D PhC/PhW device structures that are necessary for manipulation of light at the infrared wavelength (around 1550 nm)—ruled by its capability of confined light within a small volume, V. Due to the fabrication challenges and the capability of designing structures that occupy very small areas, one-dimensional PhC structures have been preferred, although there are practical performance limitations. The devices typically consist of a single row of holes embedded in a narrow single-mode photonic wire waveguide. On the other hand, photonic wire (PhW) device structures based on total internal reflection (TIR) concepts have shown a capability for reduced loss, together with less complexity. They can also provide strong optical confinement due to the large refractive index contrast between the waveguide core and its surrounding cladding, leading also to small device volumes and compact structures [35]. In addition the photonic wire approach also gives great flexibility for the design of structures such as sharp bends, abrupt Y-junctions, small device volumes, micro-cavities and Mach-Zehnder (MZ) structures [36–42]. In other words, this concept is based on high refractive index contrast where light is confined in such a narrow ridge waveguide. The combination of one-dimensional photonic crystal (PhC) structures and photonic wire (PhW) waveguides in high refractive index materials such as silicon-on-insulator (SOI) became increasingly important in a number of research areas. In order to obtain a wide range of device functionality, the reduction of propagation losses in narrow photonic wires is equally as important as enhancing the performance of the device structures.

On the other hand, 1D PhC/PhW device structures have increasingly became a topic of interest—and use a mirror design that is based on a single periodic row of holes embedded in a narrow ridge waveguide, as shown in **Figure 1**. This approach was first introduced by Foresi et al. [43]. The periodic hole mirror characteristics can be varied by changing several parameters—such as hole diameter, cavity spacing and hole spacing—as will be described in detail in Chapter 4. In the present

work, light confined within a PhC/PhW structure is directly coupled into the micro-cavity by using a tapered hole arrangement, as shown in **Figure 1**.

These kinds of device structure also have the capability of providing compact structures in small device volumes, as compared to other more complex structures such as ring resonators—which occupy larger device volumes. Furthermore, 1D PhC/PhW structures may also be preferred, since they can exhibit large band gaps as compared to what 3D photonic crystal structures can offer—thus making the PhC/PhW approach a contender for filter devices that can be integrated with other photonic devices. The fact that they share similar concepts with grating filters helps in understanding how these devices operate. With the material properties of SOI, an extremely small waveguide working in single-mode operation can be realised, with a reduction in propagation losses from 50 dB in 1996 [44] to 1.7 dB/cm in late 2006 [45], and most recently a propagation loss value of 0.91 dB/cm [46] has been achieved. The other features that have led to increasing attention to this area of research are the ability to provide a platform for the confinement of light within a small volume—for example, when a defect or a spacer is introduced between periodic mirrors. With this condition, light can be trapped within a small cavity, thus producing resonances that occur at certain frequencies within the stopband. These structures have been characterised by their high Q-factor value, adequate normalised optical transmission and small modal volume.

Maxwell's equations are important for an understanding of light propagation in photonic crystals. They are central for the solution of electromagnetic problems in dielectric media—for a variety of different lengths and dielectric scales, which are related to each other.

3. Photonic crystals: the theory

In photonic crystals, the famous Maxwell's equations are used to study light propagation in photonic crystal structure. The propagation of light in a medium is governed by the four well-known microscopic Maxwell's equations, written here in cgs units [21, 47, 48]. The microscopic forms of the Maxwell equation are given by

$$\nabla \cdot B = 0 \tag{1}$$

$$\nabla \cdot D = 4\pi\rho \tag{2}$$

$$\nabla \times E + \frac{1}{c}\left(\frac{\partial B}{\partial t}\right) = 0 \tag{3}$$

$$\nabla \times H - \frac{1}{c}\left(\frac{\partial D}{\partial t}\right) = \frac{4\pi}{c}J \tag{4}$$

or in mks/SI unit they can be written as

$$\nabla \cdot B = 0 \tag{5}$$

$$\nabla \cdot D = \rho \tag{6}$$

$$\nabla \times E + \left(\frac{\partial B}{\partial t}\right) = 0 \tag{7}$$

$$\nabla \times H - \left(\frac{\partial D}{\partial t}\right) = J \tag{8}$$

Based on Joannopoulos and Jackson [21, 47], Eqs. (1)–(4) are given in cgs units, whereas Eqs. (5)–(8) are given in mks/SI units, where the physical quantities are given as

B magnetic flux density in Tesla, T; *D* electric flux density in Coulombs per square m, C/m^2; *E* electric field strength in Volt per metre, V/m; *H* magnetic field strength in Ampere per metre, A/m; ρ electric charge density in Coulombs per cubic metre, C/m^3; J electric current density in Ampere per square metre, A/m^2.

The detailed derivation of each counterpart of Maxwell's equations is given by Jackson in Ref. [47]. For propagation in mixed dielectric medium, ρ and J are set to zero, since there are no free charges or currents in the homogeneous dielectric material. By assuming that the applied field strength is small and behave linearly, the dielectric flux density, D, can be related to the electric field density by the power series of

$$D_i = \sum_j \varepsilon_{ij} E_j + \sum_j k\chi_{ijk} E_j E_k + O\left(E^3\right) \tag{9}$$

Since the electric field strength E (r,ω) and displacement field D (r,ω) are related to the scalar dielectric constant of the microscopic and isotropic material, ε (r,ω)−χ and the higher order term can be neglected. In low loss dielectric materials, ε(r) can be treated as purely real, thus producing the electric field density written as

$$\mathrm{D(r)} = \varepsilon\ \mathrm{(r)\ E\ (r)} \tag{10}$$

In addition, for most dielectric material, the magnetic permeability, μ_r, is approximately equal to 1, giving the magnetic flux density, B, equal to the magnetic field strength, H. The flux density of the dielectric material can be written as D = ε.E where the permittivity, ε, is real. Therefore the Maxwell equation can be rewritten as already illustrated in [21, 47] as

$$\nabla \cdot H(r,t) = 0 \tag{11}$$

$$\nabla \cdot \varepsilon(r) E(r,t) = 0 \tag{12}$$

$$\nabla \times E(r,t) + \frac{1}{c}\left(\frac{\partial H(r,t)}{\partial t}\right) = 0 \tag{13}$$

$$\nabla \times H(r,t) - \frac{\varepsilon(r)}{c}\left(\frac{\partial E(r,t)}{\partial t}\right) = 0 \tag{14}$$

Then the harmonic mode of the E and H field components propagating in the dielectric medium is considered as

$$\mathrm{H(r,t)} = \mathrm{H(r)e}^{i\omega t} = 0 \tag{15}$$

and

$$\mathrm{E}(\mathrm{r},\mathrm{t}) = \mathrm{E}(\mathrm{r})\mathrm{e}^{i\omega t} = 0 \tag{16}$$

By substituting Eqs. (15) and (16) into the Maxwell equations (11)–(14), the equation is deduced to a simple condition (two divergence) as shown below:

$$\nabla \cdot H(r) = \nabla \cdot D(r) = 0 \tag{17}$$

where H(r) and E(r) and the field components at t = 0. By deriving Eqs. (15) and (16) and substituting them into Eqs. (13) and (14), the Maxwell equation will become

$$\nabla \times \left(\frac{1}{\varepsilon(r)}\nabla \times H(r)\right) = \left(\frac{\omega}{c}\right)^2 H(r) \tag{18}$$

Thus Eq. (18) derived has H components which become a master equation for dielectric medium, in particular photonic crystal with only magnetic field, H(r) component. This can also be used to recover an electric field component, E(r), of the Maxwell equation given by

$$E(r) = \left[\frac{-ic}{\omega\varepsilon(r)}\right]\nabla x H(r) \tag{19}$$

The final equation given above (18) and (19) is only used primarily to understand the basic concepts of photonic crystal (PhC) structures. These concepts can also be used for more complex structures such as 2D and 3D PhCs.

4. PhC/PhW micro-cavities

One-dimensional (1D)-PhC micro-cavities embedded in narrow photonic wire have been widely studied. A small shift in the periodic mirrors—in particular one situated in the middle of the periodic mirror—will produce a sharp resonance peak in the middle of stopband. This resonant condition oscillates naturally at certain frequencies with greater amplitudes than others within the system. The Q-factor is particularly useful in determining the qualitative behaviour of a system. For some telecom applications, such as dense wavelength division multiplexing (DWDM), the performance of those resonances is determined by their quality factors and optical transmission at a certain resonance frequency. The quality factor of a system is a dimensionless parameter that defines the first-order behaviour, for the decay, of an oscillating frequency within a micro-cavity. It is characterised by the ratio of the resonant frequency to the bandwidth of the resonance or by the decrease in the amplitude of the wave propagating through a system, within an oscillation period. Equivalently, it compares the frequency at which the system oscillates to the rate of energy dissipated by the system. A higher Q-factor value indicates a lower rate of energy dissipation relative to the oscillation frequency, so the oscillations die out more slowly. For example, a pendulum suspended from a high-quality bearing, oscillating in air, would have a high *Q*, while a pendulum immersed in oil would have a low one. In optics, the Q-factor is generally given by [49, 50]:

$$Q = \frac{2\pi f_0 E}{P} \tag{20}$$

where ε is the stored energy in the cavity and P is the power dissipated within the cavity, given by

$$P = -\frac{dE}{dt} \tag{21}$$

The Q-factor is equal to the ratio of the resonant frequency to the bandwidth of the cavity resonance shown in **Figure 2**.

Ideally, the average lifetime of a resonant photon in the cavity is proportional to the cavity's *Q*. Resonant systems respond to frequencies close to their natural frequency much more strongly than they respond to other frequencies. A system with a high *Q* resonates with greater amplitude (at the resonant frequency) than one with a low *Q*-factor, and its response falls off more rapidly as the frequency moves away from resonance. Therefore the physical interpretation of resonance is given by its general equation:

$$Q = \frac{f_0}{\Delta f} \tag{22}$$

where f_0 is the central frequency of the resonance and Δf is the frequency difference within at 3 dB points or ½ of the total energy stored in the micro-cavity system. In this present work, several different types of resonator have been studied, namely, waveguide Bragg gratings and 1D PhC/PhW waveguides—as shown in **Figure 3**. Unlike the Bragg grating waveguide [51], which has a rectangular recess embedded on a photonic wire waveguide, a single row of holes is used as a set of mirrors.

This structure consists of a single row of holes drilled in the 500 nm width of wire waveguides. Those holes acted as a periodic mirror where light impinging on the PhC bounced back provide a band gap where light is forbidden to propagate at certain frequency. A spacer was introduced symmetrically between the periodic mirrors—thus producing a narrow resonance in the transmission. The concepts for this kind of structure were proposed by Krauss and Foresi [5, 20]. But the Q-factor at this [43] resonance condition obtained was small (~500). The PhC hole mirrors resulted in a wide stopband (approximately 182 nm), using eight PhC mirrors holes, whereas 32 period waveguide Bragg gratings were used and showed a narrower stopband of approximately 88 nm. This difference is due to the fact that the light was coupled more strongly in the periodic hole mirrors—where 95% of the light was reflected with the periodic hole arrangement, as compared to the waveguide Bragg

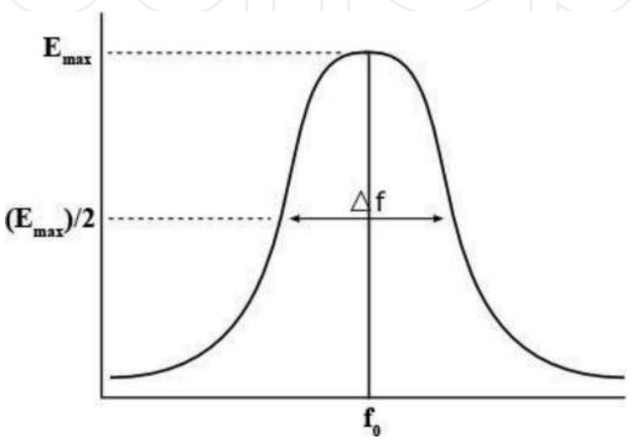

Figure 2.
A typical resonance frequency resulted from micro-cavity structures defined by the central resonance frequency, f_o, and the bandwidth of the frequency at 3 dB points (energy at the steady state condition).

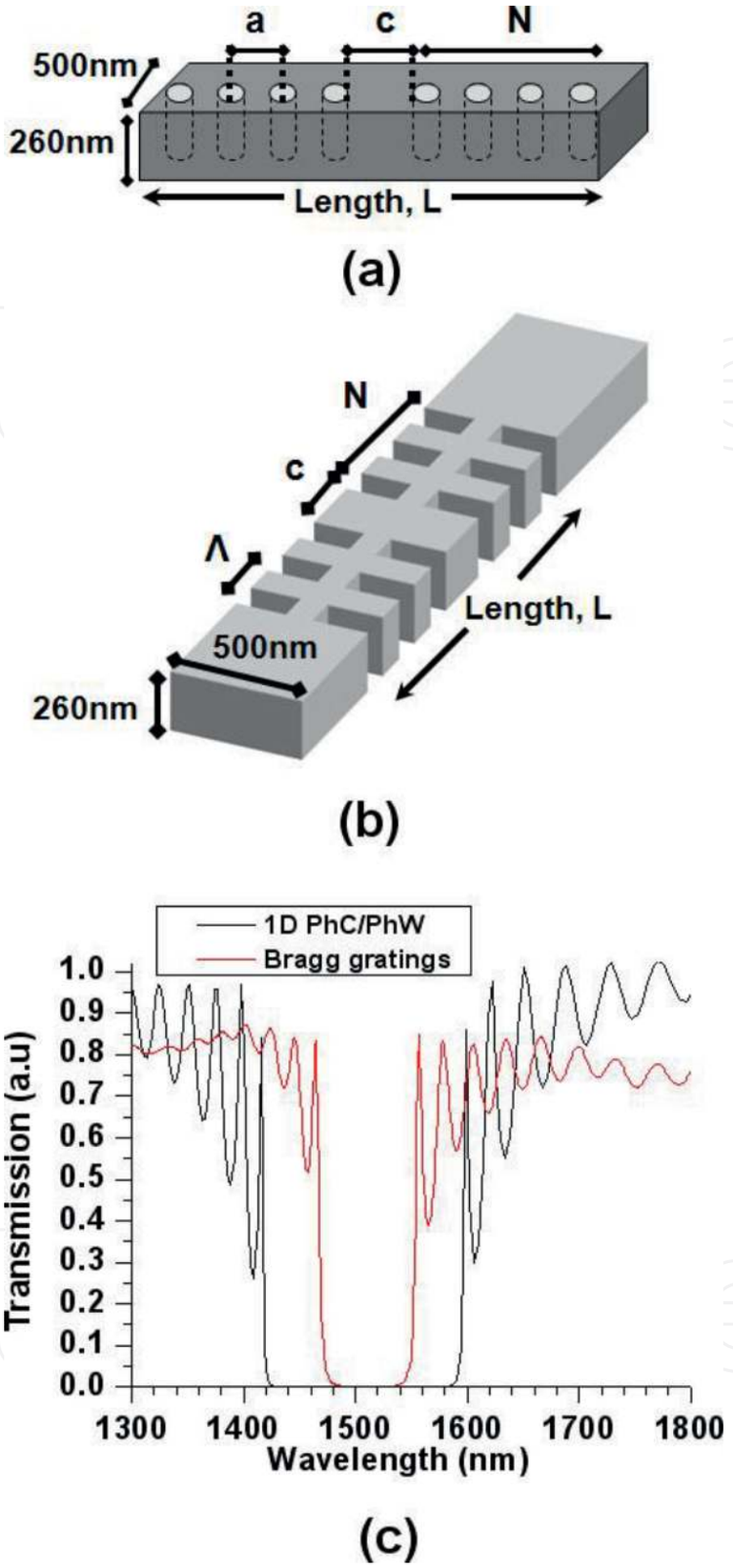

Figure 3.
Different types of PhW waveguides micro-cavity. (a) 1D PhC/PhW waveguides with cavity length (distance between two hole edges of the hole spacer) c, hole periodic spacing (distance between centre-to-centre hole), a and number of periodic holes, N (b) PhW Bragg gratings waveguides with cavity length, c, period, Λ, and number of recess period, N, and (c) transmission spectra of Bragg grating waveguides and 1D PhC/PhW.

gratings where ~82% light was reflected back. Hole gratings show more pronounce stopbands compared to their counterpart. As mentioned before, stronger reflection was observed for the hole grating. The hole gratings have a bigger stopband of

approximately 180 nm, which is useful for some filter designs and some optical communications applications. This wide stopband may be compared with the limited bandwidth of the stopband or may be contrasted with the significantly smaller stopband of the rectangular recess grating.

In addition, for this grating condition, the total length, L, of the waveguide Bragg grating of ~11 μm is longer by a factor of four in order to achieve a practical stopband spectrum, as compared with the hole grating structures (~3 μm). The present work will demonstrate the design, fabrication and characterisation of the 1D PhC-based micro-cavity, which is potentially useful for wavelength division multiplexing (WDM) in PhC devices. A single row of PhC holes is embedded in a narrow photonic wire waveguide to allow sufficient optical coupling for integration with other photonic devices. This thesis will address the importance of using a combination of hole tapering with a different hole diameter at the interface between the un-patterned wire and the cavity mirror, as well into the micro-cavity region—in order to achieve large optical transmission together with a high-resonance Q-factor value. Achieving high Q-factor together with large optical transmission remains a significant challenge. The key points towards designing an ultrahigh Q-factor device that confines light in such a small volume lie in reducing the modal mismatch between the un-patterned wire and the PhC or grating sections. Therefore, designing a tapered structure to reduce the modal mismatch at the interfaces between the mirror region and the PhW waveguide sections is necessary. One of the approaches used to overcoming this situations is the use of a taper structure consisting of holes with different sizes through progressive increase of the hole size into the mirror region [52]. On the other hand, the same model has also been used with short taper sections incorporated into a 1D micro-cavity-based system [53]. Using these concepts, the impact of progressive tapering using different hole diameters has shown a huge improvement in enhancing the quality factor of the micro-cavity [54, 55].

Therefore, 1D PhC/PhW micro-cavities can provide higher optical confinement in smaller volumes that are closer to the theoretical value of 0.055 $(\lambda/n)^3$ [54]—which has a great potential in high-index contrast materials such as silicon-on-insulator (SOI) to be used in some telecommunication applications such as DWDM, add-drop filter switching experiments, slow light and non-linear optics.

5. The finite-difference time-domain (FDTD) approach

There have been several methods used for computational purposes, especially for modelling photonic crystal structures and photonic wire waveguides. The finite-difference time-domain (FDTD) approach is a commonly used technique because it provides both the spatial and temporal properties of the structure with a single calculation, making it suitable for the analysis of many structures. However it requires a lot of time to compute a single run. This technique uses the famous Maxwell's equations based on the Yee mesh [56], published in 1966. Yee has proposed this technique in order to derive a numerical scattering problem and electromagnetic absorption on the basis of Maxwell's equations. The computational domain was first established, in order to determine the physical region within which the calculation will be performed. The electric field, E, and the magnetic field, H, are distinguished at every point within the domain by specifying the material used at each domain point (in *xyz* directions). The materials involved could be free space (air), metal or dielectric material. A light source in the form of a plane wave is then impinging on the chosen material. Later in 1994, the technique called the perfectly matched layer (PML) boundary condition was introduced [57]. It was

used as an absorption mechanism for electromagnetic wave incident on the edge of the computational domain in space. The FDTD method can be implemented in either 2D or 3D computations—but it requires a lot of memory and power consumption for a single computational run, especially for a large device in 3-D. 2D FDTD reduces time and memory requirement significantly. It employs a refractive index approximation or average refractive index of the slab—called effective index method (EIM). By using this method, the cross-sectional index profile is usually transformed to the one-dimensional index profile by using EIM [58, 59]. In the EIM approach, the eigenvalue of the equivalent slab waveguide is an approximate index value of the original waveguide. Although the EIM approach provides a good approximation, it still suffers from errors in the vicinity of the cut-off [60–63]. At the beginning of this present work, this method is used to investigate the preliminary behaviour of the device with the assumption that losses are negligible. In order to reduce simulation time and power consumption, 2D FDTD approach was initially used throughout the course to analyse the general optical behaviour of the device structures—implementing EIM. Since EIM method is only an approximation of the actual refractive index obtained by taking into account the whole ridge waveguide structures, at least a small discrepancy between the simulations measured results is very much to be expected. On the other hand, the 3D FDTD method can give a better estimate of the properties, although it is time- and power-consuming, which is still a major concern.

During this present work, different types of commercial software have been used. The Fullwave RSoft computational software has been used at the beginning of this work, where only 2D computation was deeply explored due to the longer time and high power consumption for 3D FDTD. Based on the concept proposed by Yee [56], several key pieces of information are needed to solve the basic propagation problem in optical waveguide which comprised of:

- The refractive index distribution, n(x,y,z)
- Electromagnetic field excitation (plane wave or Gaussian)
- Finite computational domain in x, y and z direction
- The boundary of PML layer
- Spatial grid size, Δx and Δy
- Time step, Δt, and the total length of the simulation time

For 2D FDTD computation, the average refractive index, n, or effective index, n_{eff}, of the slab waveguide of a material is used rather than the actual refractive of that particular material. This can be obtained using mode-matching method available in the Fimm-wave® commercial software by Photon Design®. This method includes the approximation of refractive index in both propagation direction of vertical and horizontal confinement of the slab waveguide. The transverse section of the device is first simulated using Fimm-wave® simulation tools. It shows the intensity of light in guiding mode, confinement of light inside the slab and the effective index, n_{eff}. It also shows the leaky region where light is not confined inside the slab. **Figure 4** shows the contour plot of the TE fundamental mode of the waveguide. It shows the intensity of light confinement along the core at 1.52 μm wavelength at different etching depths. It is suggested that the different etching depths will give rise to the abrupt change of the effective index, n_{eff}, at the

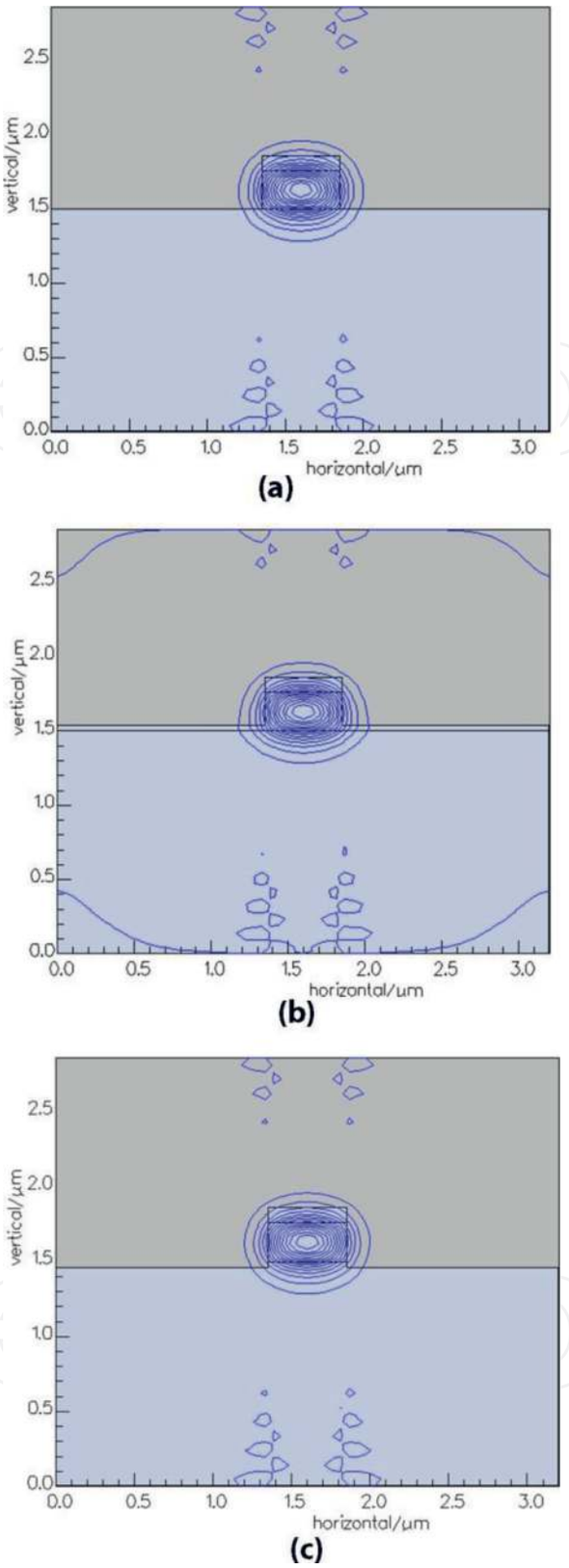

Figure 4.
Contour plot of the TE fundamental mode intensity. (a) Fully etched. (b) Shallow etched. (c) Deep etched.

boundary of silicon core and silica cladding (lower cladding) where some of the light are reflected back into the cladding (backscattering). This can be improved by etching slightly deeper into the lower cladding by around 20–40 nm, thus reducing scattering losses. The effective index calculated using the Fimm-wave™ simulation tool for 500 nm wide ridge waveguides at different etching depths is given in **Figure 4(a)** and **(b)**. More profound field intensity is obtained for fully etched

silicon where symmetric field distribution is obtained (see **Figure 4(a)**) as compared to shallow- and deep-etched silicon.

Depositing silica on top of the photonic wire can also improve the confinement of TE fundamental mode of the photonic wire significantly. From **Figure 5**, 100, 200 and 400 nm SiO_2 have been deposited on the photonic wire. But to reduce the device preparation complexity and process development, the slab waveguide design based on fully etched silicon is considered throughout this work. The calculated n_{eff} based on this design is 2.97, which will be used for 2D FDTD computation.

The value of n_{eff} is fed into the full-wave simulation tool by using either pulsed or continuous Gaussian source for slab waveguide. The finite computational domain is optimised in space covering the area between 10 and 20 μm in length and 2 μm in

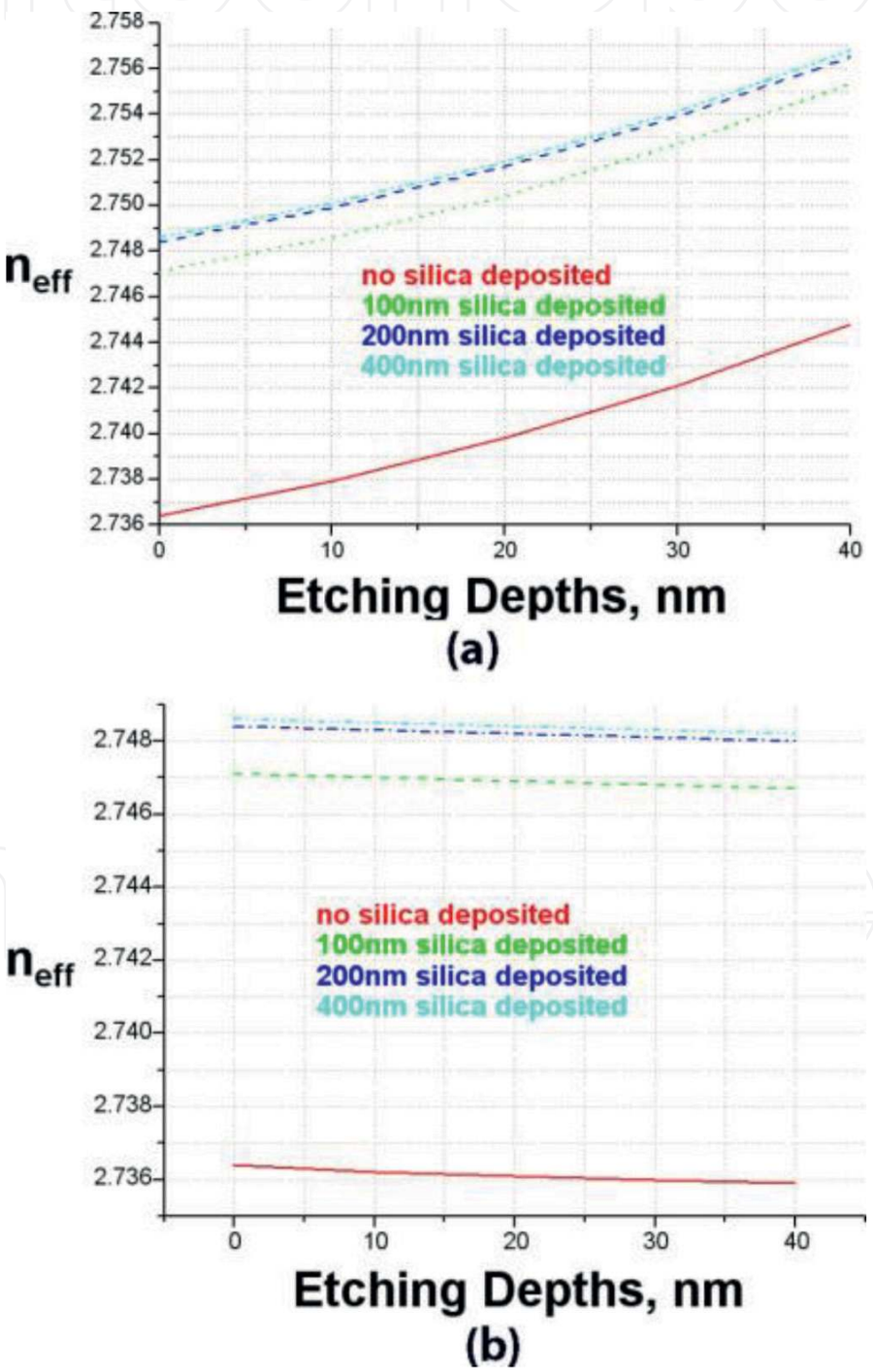

Figure 5.
The effective index, n_{eff}, at different etching depths for symmetric (silica deposition on top) and asymmetric waveguide (no silica deposition). (a) Shallow etched. (b) Deep etched.

width since large computational area will contribute to a longer simulation time and also consume more memory and power.

The space must be exactly proportionate to the size of the optical waveguide. The thickness of PML required for the device operating at around 1.52 μm wavelength is 0.5 μm to provide better electromagnetic wave absorption at the boundary. Other parameters that contribute to the accuracy of the simulation are determined by the choice of the spatial grid or mesh size, where smaller grid spacing gave more accurate computation. In other words, the closer the resolution in simulation to the actual device, the more accurate simulation will be established.

During the second half of the computational process, the author has used other commercially available software to compute all the device structures. This software is found to be more accurate than the previous simulation tool. On the other hand, by using the same parameters in the crystal wave tool as previously used in full-wave, the simulation time has been reduced by a factor of five, and the result obtained is closer to the measured result as shown in one of the example in **Figure 6**. The comparison is made by using 12-period 1D PhC mirrors with diameters of 350 nm and periodic spacing of 360 nm. By looking at the band edge location of the measured result in **Figure 6**, the 2D FDTD crystal wave shows closer result (band edge) than the one computed using RSoft tools where the deviation of 83 nm is observed between the simulation and the measured result. But this is understood to be due to small deviation in the dimension of the structures produced after fabrication process as real devices.

No further investigation is made in reference to the discrepancy between the different examples of commercial software, but the problem has been addressed to the relevant personnel. As a result, based on further tests carried out using different measurements run to compare the results with the simulation, the CrystalWave software have been chosen as the relevant tools that are well-suited to the design structures used throughout this present work.

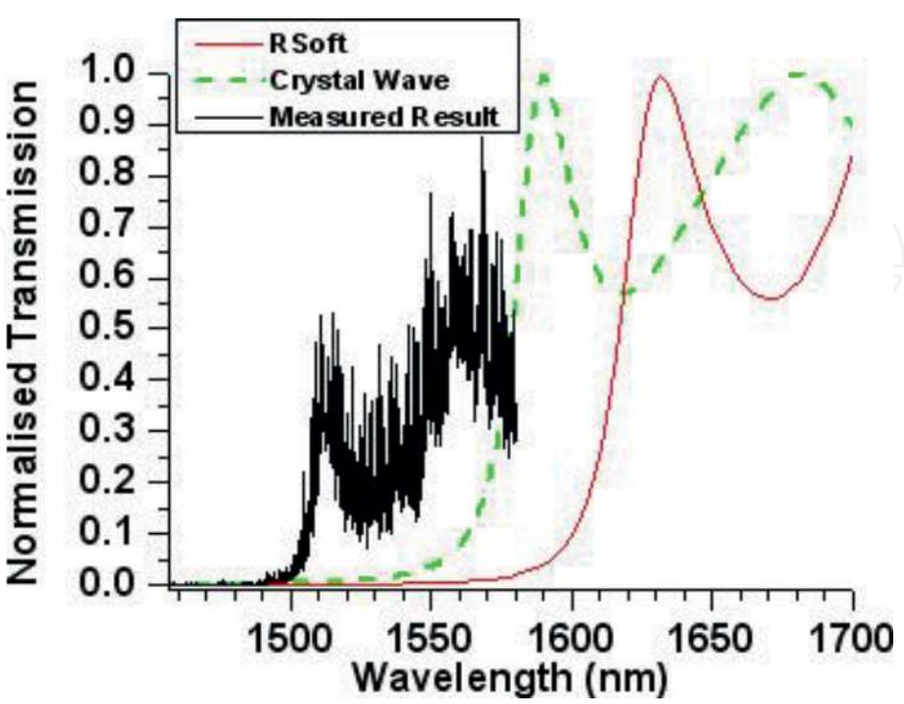

Figure 6.
An example showing a comparison between 2D FDTD computed using different simulations tools (RSoft and crystal wave) with the measured result.

6. Conclusion

In conclusion, the 2D simulation approach is used to produce preliminary designs for the device, together with the employment of an effective index approximation based on the waveguide properties of the base material structure discussed earlier. 2D simulation helps with obtaining a better understanding of the general behaviour of the device—but 3D simulation gives more accurate prediction of the results, at the expense of much greater time and energy consumption. Both 2D and 3D simulations were carried out using the commercial software using finite-difference time-domain (FDTD) approach. This chapter in particular demonstrated the detailed theoretical models of single-row PhC cavities embedded in narrow (typically 500 nm wide) photonic wire waveguides based on silicon-on-insulator (SOI). The device structures have been designed to operate in TE polarisation at wavelengths around 1550 nm. The compactness together with high reflectivity and possibilities for an active tuning capability make the device suitable as a basic building block for incorporation into integrated circuits where several functions are realised on a single chip—i.e. what are commonly known as high-density photonic integrated circuits (PICs). On the other hand, it may also be useful in providing one of the solutions for the design of compact filters for either coarse or dense wavelength division multiplexing situations, for high-speed switching and non-linear optics. For instance, FDTD approach used in this chapter has shown a significantly good agreement with the measured result—thus it can be used as a method to obtain a preliminary result before the actual design for fabrication is proposed.

Author details

Ahmad Rifqi Md Zain[1,2*] and Richard M. De La Rue[3]

1 Institute of Microengineering and Nanoelectronics, University Kebangsaan Malaysia (UKM), Bangi, Selangor, Malaysia

2 John Mc Kay Lab, School of Engineering and Applied Science (SEAS), Harvard University, Cambridge, MA, United States

3 Schoolf of Engineering, University of Glasgow, Glasgow, United Kingdom

*Address all correspondence to: rifqi@ukm.edu.my

References

[1] Miller SE. Integrated optics: An introduction. Bell System Technical Journal. 1969;**48**:2059-2070

[2] Yariv A, Leite RCC. Dielectric-waveguide mode of light propagation in p-n junctions. Applied Physics Letters. 1963;**2**:55

[3] Bond WL, Cohen BG, Leite RCC, Yariv A. Observation of the dielectric - waveguide mode of light propagation in p-n junctions. Applied Physics Letters. 1963;**2**:57

[4] Nelson DF, Reinhardt FK. Light modulation by the electro optic effect in reverse-biased GaP p-n junction. Applied Physics Letters. 1964;**5**:148

[5] Nathan MI, Dumke WD, Burns G, Dill FH Jr, Lasher G. Stimulated emission of radiation from GaAs p-n junction. Applied Physics Letters. 1962; **1**:62

[6] Basov NG, Vul B, Popov YuM. Zhurnal Eksperimentalnoi i Teoreticheskoi Fizik. 1959;**37**;587-588. [Sov. Phys.—JETP. 1960;**10**:416]

[7] Maiman TH. Stimulated optical radiation by ruby lasers. Nature. 1960; **187**:493

[8] Hall RN, Fenner GE, Kingsley JD, Soltys TJ, Carlson RO. Coherent light emission from GaAs junction. Physical Review Letters. 1962;**9**:366-368

[9] Kogelnik H. An introduction to integrated optics. IEEE Transactions on Microwave Theory and Techniques. 1975;**23**(1):2-16

[10] Adams MJ, Steventon AG, Devlin WJ, Henning ID. Semiconductor lasers for long-wavelength optical fibre communications systems. IEE Materials and Devices Series 4. US: Peter Peregrinus; 1987.

[11] Quist TM, Rediker RH, Keyes RJ, Krag WE, Lax B, McWhorter AL, et al. Semiconductor maser of GaAs. Applied Physics Letters. 1962;**1**:91

[12] Purcell EM, Torrey HC, Pound RV. Resonance absorption by nuclear magnetic moments in a solid. Physical Review. 1946;**69**:37

[13] Purcell EM. Spontaneous emission probabilities at radio frequencies. Physical Review Letters. 1946;**69**:681

[14] John S. Strong localization of photons in certain disordered dielectric superlattices. Physical Review Letters. 1987;**58**(23):2486-2489

[15] Yablonovitch E. Inhibited spontaneous emission in solid-state physics and electronics. Physical Review Letters. 1987;**58**(20):2059-2062

[16] Soref RA, Lorenzo JP. All-silicon active and passive guided-wave components for λ = 1.3 μm and 1.6 μm. IEEE Journal of Quantum Electronics. 1986;**22**(6):873-839

[17] Jalali B, Yegnanarayanan S, Yoon T, Yoshimoto T, Rendina I, Coppinger F. Advances in silicon-on-insulator optoelectronics. IEEE Journal of Selected Topics in Quantum Electronics. 1998;**4**(6):938-947

[18] Masini G, Colace L, Assanto G. Si based optoelectronics for communications. Material Science and Engineering B. 2002;**89**:2-9

[19] Krauss TF, De la Rue RM. Photonic crystals in the optical regime—Past, present and future. Progress in Quantum Electronics. 1999;**23**:2

[20] Krauss TF. Planar photonic crystal waveguide devices for integrated optics.

Physica Status Solidi A—Applied Research. 2003;**197**(3):688-702

[21] Joannopoulos JD, Meade RD, Winn JN. Photonic Crystals Molding the Flow of Light. Princeton, US: Princeton University Press; 1995

[22] Scherer A, Painter O, Vuckovic J, Loncar M, Yoshie T. Photonic crystals for confining, guiding, and emitting light. IEEE Transactions on Nanotechnology. 2002;**1**(1):4-11

[23] Yoshie T, Vuckovic J, Scherer A, Chen H, Deppe D. High quality two-dimensional photonic crystal slab cavities. Applied Physics Letters. 2001; **79**(26):4289-4291

[24] Park H-G, Hwang J-K, Huh J, Ryu H-Y, Lee Y-H, Kim J-S. Nondegenerate monopole-mode two-dimensional photonic band gap laser. Applied Physics Letters. 2001;**79**(19):3032-3034

[25] Painter O, Vuckovic J, Scherer A. Defect modes of a two-dimensional photonic crystal in an optically thin dielectric slab. Journal of the Optical Society of America B. 1999;**16**(2): 275-285

[26] Ryu H-Y, Notomi M, Lee Y-H. High-quality-factor and small-mode-volume hexapole modes in photonic-crystal-slab nanocavities. Applied Physics Letters. 2003;**83**(21):4294-4296

[27] Jin C, Fan S, Han S, Zhang D. Reflectionless multichannel wavelength demultiplexer in a transmission resonator configuration. IEEE Journal of Quantum Electronics. 2003;**39**(1): 160-165

[28] Chong H, De La Rue RM. Planar photonic crystal microcavities for add/drop filter functionality. In: Post-deadline Paper for 11th European Conference on Integrated Optics (ECIO 2003); Prague, Czech Republic. 2003

[29] Lin SY, Chow E, Johnson SG, Joannopoulos JD. Direct measurement of the quality factor in a two-dimensional photonic-crystal microcavity. Optics Letters. 2001; **26**(23):1903-1905

[30] Loncar M, Nedeljkovic D, Doll T, Vuckovic J, Scherer A, Pearsall T. Waveguiding in planar photonic crystals. Applied Physics Letters. 2000; **77**(13):1937-1939

[31] Olivier S, Benisty H, Smith CJM, Rattier M, Weisbuch C, Krauss TF. Transmission properties of two-dimensional photonic crystal channel waveguides. Optical and Quantum Electronics. 2002;**34**:171-181

[32] Notomi M, Shinya A, Yamada K, Takahashi J, Takahashi C, Yokohama I. Singlemode transmission within photonic bandgap of width-varied single-line-defect photonic crystal waveguides on SOI substrates. Electronics Letters. 2001;**37**(5):293-295

[33] O'Faolain L et al. Low loss propagation in photonic crystal waveguide. Electronic Letters. 2006; **25**:42

[34] Armani DK, Kippenberg TJ, Spillane SM, Vahala KJ. Ultralow-threshold microcavity Raman laser on a microelectronic chip. Nature. 2003;**421**: 925

[35] Bogaerts W, Taillaert D, Luyssaert B, Dumon P, Van Campenhout J, Bienstman P, et al. Basic structures for photonic integrated circuits in silicon-on-insulator. Optics Express. 2004;**12**(8): 1583-1591

[36] Ahmad RU, Pizzuto F, Camarda GS, Espinola RL, Rao H, Osgood RM. Ultracompact corner-mirrors and T-branches in silicon-on-insulator. IEEE Photonics Technology Letters. January, 2002;**14**(1):65-67

[37] Ohno F, Fukuzawa T, Baba T. Mach-Zehnder interferometers composed of μ-bends and μ-branches in a Si photonic wire waveguide. Japanese Journal of Applied Physics. 2005;**44** (7A):5322-5323

[38] De La Rue R, Chong H, Gnan M, Johnson N, Ntakis I, Pottier P, et al. Photonic crystal and photonic wire nano-photonics based on silicon-on-insulator. New Journal of Physics. 2006; **8**:256

[39] Camargo EA, Chong HMH, De La Rue RM. Highly compact asymmetric Mach-Zehnder device based on channel guides in a two-dimensional photonic crystal. Applied Optics. 2006;**45**: 6507-6510

[40] Camargo EA, Chong HMH, De La Rue RM. Four-port coupled channel-guide device based on 2D photonic crystal structure. Photonics and Nanostructures—Fundamentals and Applications. 2004;**2**(3):207-213

[41] Zhang H, Gnan M, Johnson NP, De La Rue RM. Ultra-small Mach-Zehnder interferometer devices in thin silicon-on-insulator. In: Integrated Photonics Research and Applications (IPRA); Uncasville, Conn., USA. 2006

[42] Zhao CZ, Li GZ, Liu EK, Gao Y, Liu XD. Silicon-on-insulator Mach-Zehnder wave-guide interferometers operating at 1.3 μm. Applied Physics Letters. 1995; **67**(17):1735

[43] Foresi JS, Villeneuve PR, Ferrera J, Thoen ER, Steinmeyer G, Fan S, et al. Photonic bandgap microcavities in optical waveguides. Nature. 1997;**390**: 143-145

[44] Sakai A, Hara G, Baba T. Propagation characteristics of ultrahigh-delta optical waveguide on silicon-on-insulator substrate. Japanese Journal of Applied Physics Letters. 2001;**40**(4B): L383-L385

[45] Xia F, Sekaric L, Vlasov YA. Ultracompact optical buffers on a silicon chip. Nature Photonics. 2007;**1**(1):65-71

[46] Gnan M, Thoms S, Macintyre DS, De La Rue RM, Sorel M. Fabrication of low-loss photonic wires in silicon-on-insulator using hydrogen silsesquioxane electron-beam resist. Electronics Letters. 2008;**44**:115-116

[47] Jackson JD. Classical Electrodynamics. New York: John Wiley; 1962

[48] Jackson JD. Classical Electrodynamics. 3rd ed. New York: Wiley; 1998. p. 177

[49] Jackson RG. Novel Sensors and Sensing. CRC Press; 2004. p. 28. ISBN 075030989X

[50] Crowell B. Vibrations and Waves. Light and Matter Online Text Series. 2006. Ch. 2

[51] Gnan M, Bellanca G, Chong HMH, Bassi P, De La Rue RM. Modelling of photonic wire Bragg gratings. Optical and Quantum Electronics. 2006;**38** (1–3):133-148

[52] Lalanne P, Talneau A. Modal conversion with artificial materials for photonic-crystal waveguides. Optics Express. 2002;**10**:354-359

[53] Peyrade D, Silberstein E, Lalanne P, Talneau A, Chen Y. Short Bragg mirrors with adiabatic modal conversion. Applied Physics Letters. 2002;**81**: 829-831

[54] Velha P, Rodier JC, Lalanne P, Hugonin JP, Peyrade D, Picard E, et al. Ultra high reflectivity photonic bandgap mirrors in a ridge SOI waveguide. New Journal of Physics—IOPscience. 2006; **8**(204):1-13

[55] Lalanne P, Hugonin JP. Bloch-wave engineering for high-Q, small-V

microcavities. IEEE Journal of Quantum Electronics. Nov. 2003;**39**(11): 1430-1438

[56] Yee KS. Numerical solution of initial boundary value problems involving Maxwell's equations in isotropic media. IEEE Transactions on Antennas and Propagation. 1966;**14**:302-307

[57] Berenger JP. A perfectly matched layer for the absorption of electromagnetic waves. Journal of Computational Physics. 1994;**114**(2): 185-200

[58] Buus J. The effective index method and its application to semiconductor lasers. IEEE Journal of Quantum Electronics. 1982;**18**(7):1083-1089

[59] Chung Y, Dagli N. An assessment of finite difference beam propagation method. IEEE Journal of Quantum Electronics. Aug. 1990;**26**(8):1335-1339

[60] Cheng YH, Lin WG. Investigation of rectangular dielectric waveguides: An iteratively equivalent index method. IEE Proceedings. 1990;**137**(5):323-329

[61] Furuta H, Noda H, Ihaya A. Novel optical waveguide for integrated optics. Applied Optics. 1974;**13**:323-326

[62] Kumar A, Thyayarajan K, Ghatak AK. Analysis of rectangular core dielectric waveguide: An accurate perturbation approach. Optics Letters. 1983;**8**:63-65

[63] Kim CM, Jung BG, Lee CW. Analysis of dielectric rectangular waveguide by modified effective index method. Electronic Letters. 1986;**22**(6): 296-298